Convolutional Tensor-Train LSTM for Spatio-temporal Learning

Jiahao Su [*,1,2] **Wonmin Byeon** [*,3] **Furong Huang** [4] **Jan Kautz** [3] **Animashree Anandkumar** [3]

Abstract

Higher-order Recurrent Neural Networks (RNNs) are effective for long-term forecasting since such architectures can model higher-order correlations and long-term dynamics more effectively. However, higher-order models are expensive and require exponentially more parameters and operations compared with their first-order counterparts. This problem is particularly pronounced in multi-dimensional data such as videos. To address this issue, we propose *Convolutional Tensor-Train Decomposition (CTTD)*, a novel tensor decomposition with convolutional operations. With CTTD, we construct *Convolutional Tensor-Train LSTM (Conv-TT-LSTM)* to capture higher-order space-time correlations in videos. We demonstrate that the proposed model outperforms the conventional (first-order) Convolutional LSTM (ConvLSTM) as well as other ConvLSTM-based approaches in pixel-level video prediction tasks on Moving-MNIST and KTH action datasets, but with much fewer parameters.

1. Introduction

Video understanding is a challenging problem, as it requires a model to learn complex representation of spatial and temporal dynamics. The problem arises in a wide range of applications, including autonomous driving, robot control (Finn & Levine, 2017), and other visual perception tasks like action recognition or object tracking (Alahi et al., 2016).

Recurrent Neural Network (RNN, especially LSTM) and Transformer are common choices to learn temporal dynamics (Hochreiter & Schmidhuber, 1997; Vaswani et al., 2017). These models are extended to learn spatio-temporal data by incorporating convolution operations (Convolutional LSTM (Xingjian et al., 2015)) or attention in spatiotemporal volumes (Video Transformer (Weissenborn et al., 2019)). While Transformer directly maps input and output sequences using attention mechanism, RNNs encodes the sequential dependencies by the interactions of consecutive two steps (first-order Markovian model).

Higher-order RNNs (Soltani & Jiang, 2016; Yu et al., 2017) are their higher-order Markovian generalization that explicitly characterize long-term temporal dependencies. These models are effective in long-term forecasting problems by incorporating higher-order states (longer history) in RNNs: at each time step, a model learns longer-term correlations from multiple past steps. Although Transformer can also be used to capture long-term dependencies, it is hard to design a model especially for multi-dimensional data. Higher-order RNNs learn underlying sequential correlations which makes Markovian models more natural for sequence forecasting problems.

The transition dynamics in higher-order RNNs is naturally characterized by higher-order tensors (instead of transition matrices as in first-order models) with the order equal to the number of past steps for prediction. Therefore, these models typically require exponentially more parameters and operations than their first-order counterparts, making the learning harder and prone to overfitting.

A principled approach to address the curse of dimensionality is *tensor decomposition*, where a higher-order tensor is compressed into smaller core tensors (Anandkumar et al., 2014). Tensor representations are powerful since they retain rich expressivity even with a small number of parameters. The synergy of tensor method and higher-order RNNs has led to compressed *higher-order tensor RNNs* (Yu et al., 2017), where the transition tensor is factorized by *Tensor-Train Decomposition* (TTD) (Oseledets, 2011).

However, this approach is not directly compatible to learning in videos since classic decompositions do not preserve the spatio-temporal structure. To extend higher-order RNNs to video applications, we propose a novel *Convolutional Tensor-Train Decomposition (CTTD)*, which is capable of factorizing an intractably large convolutional operator into a set of smaller components.

[*] Equal contribution [1] This work was done while the author was an intern at NVIDIA. [2] Department of Electrical and Computer Engineering, University of Maryland, College Park [3] NVIDIA Research, NVIDIA Corporation, Santa Clara [4] Department of Computer Science, University of Maryland, College Park. Correspondence to: Jiahao Su <jiahaosu@terpmail.umd.edu>, Wonmin Byeon <wbyeon@nvidia.com>.

Many recent video models use *Convolutional LSTM (ConvLSTM)* as a basic block in RNNs (Xingjian et al., 2015), where spatio-temporal information is encoded as a tensor explicitly in each cell. Like the traditional RNNs, the model is in nature a first-order Markovian model. Therefore, the model cannot easily capture higher-order temporal correlations. Most of first-order ConvLSTM-based approaches focus on next or first few frames prediction (Lotter et al., 2016; Finn et al., 2016; Byeon et al., 2018).

With CTTD, we propose a higher-order generalization to ConvLSTM, *Convolutional Tensor-Train LSTM (Conv-TT-LSTM)*, that is able to learn long-term spatio-temporal structure in videos. We show experimentally that our proposed Conv-TT-LSTM outperforms the plain ConvLSTM and other ConvLSTM-based models augmented by other techniques (Finn et al., 2016; Wang et al., 2017; 2018a) and achieve the state-of-the-art in long-term video prediction.

Contributions. We propose *Convolutional Tensor-Train LSTM* (Conv-TT-LSTM), a higher-order RNN that effectively learns long-term spatio-temporal dynamics.

- We introduce a novel *Convolutional Tensor-Train Decomposition* (CTTD) that is capable to factorize a large convolutional kernel into a chain of smaller tensors.
- We integrate CTTD into convolutional LSTM (ConvLSTM) and propose Conv-TT-LSTM, which learns higher-order spatio-temporal correlations in video sequence with a small number of model parameters.
- We address the problem of gradient instability in training higher-order tensor RNNs, by carefully designing learning scheduling and gradient clipping.
- In the experiments, we show our proposed Conv-TT-LSTM consistently produces sharper prediction over a long period of time than first-order ConvLSTM for both Moving-MNIST-2 and KTH action datasets. In addition, Conv-TT-LSTM outperforms the state-of-the-art PredRNN++ (Wang et al., 2018a) in LPIPS (Zhang et al., 2018) by 0.050 on the Moving-MNIST-2 and 0.071 on the KTH action dataset, with 5.6 times fewer parameters.

In summary, we obtain best of both worlds: capturing higher-order spatio-temporal correlations and model compression.

2. Related Work

Tensor Decomposition. In machine learning, tensor decompositions, including *CP decomposition* (Anandkumar et al., 2014), *Tucker decomposition* (Kolda & Bader, 2009), and *Tensor-Train decomposition* (Oseledets, 2011), are widely used for dimensionality reduction (Cichocki et al., 2016) and learning probabilistic models (Anandkumar et al., 2014). In deep learning, prior works focused on their application in model compression, where the tensors of model parameters are factorized into smaller tensors. This technique has been used in compressing convolutional networks (Lebedev et al., 2014; Kim et al., 2015; Novikov et al., 2015; Su et al., 2018; Kossaifi et al., 2017; Kolbeinsson et al., 2019; Kossaifi et al., 2019), recurrent networks (Tjandra et al., 2017; Yang et al., 2017) and transformers (Ma et al., 2019).

Tensor Recurrent Neural Networks (Tensor RNNs). Tensor methods have been used to compresse recurrent networks in diverse aspects: **(1)** Sutskever et al. (2011) introduces *multiplicative RNNs*, where the weights tensor for inputs-states interactions are factorized into three matrices. **(2)** Yu et al. (2017) uses tensor-train decomposition to constrain the complexity of higher-order LSTM, where each step is computed based on the outer product of previous steps. While this work only considers vector input at each step, we generalize their approach to higher-order ConvLSTM to cope with video input using our proposed Convolutional Tensor-Train Decomposition. **(3)** Yang et al. (2017) has proposed to compress both inputs-states and states-states matrices within each cell with Tensor-Train decomposition by reshaping the matrices into tensors, and showed improvement in video classification. Different from Yang et al. (2017), we aim to compress higher-order ConvLSTM (instead of first-order fully-connected LSTM). Furthermore, we propose Convolutional Tensor-Train decomposition to deal with a dense prediction problem, which requires the decomposition to preserve spatial structure after compression.

Higher-order RNNs Zhang et al. (2016) and Soltani & Jiang (2016) introduce connections cross multiple previous time steps to better learn long-term dynamics. These models require excessively more parameters than first-order RNNs. Yu et al. (2017) addressed the problem by compressing the model parameters using Tensor-Train Decomposition.

Video Prediction. Prior works on video prediction have focused on several directions: predicting short-term video (Lotter et al., 2016; Byeon et al., 2018), decomposing motion and contents (Finn et al., 2016; Villegas et al., 2017; Denton et al., 2017; Hsieh et al., 2018), improving the objective function (Mathieu et al., 2015), and handling diversity of the future (Denton & Fergus, 2018; Babaeizadeh et al., 2017; Lee et al., 2018). Many of these works use ConvLSTMas a base module, which deploys 2D convolutional operations in LSTM to efficiently exploit spatio-temporal information. Some works modified the standard ConvLSTM to better capture spatio-temporal correlations (Wang et al., 2017; 2018a). Wang et al. (2018b) integrated 3D convolutions into ConvLSTM. In addition, current cell states are combined with its historical records using self-attention to efficiently recall the history information. Byeon et al. (2018) applied ConvLSTM in all possible directions to capture full contexts in video. They also demonstrated strong performance using a deep ConvLSTM network as a baseline, which is used as the base architecture in the present paper.

3. Tensor Diagrams and Tensor Operations

In this section, we introduce the basic concepts of *tensor diagrams* and *tensor operations*. These concepts will serve as building blocks for higher-order models (in particular, tensor-train models) in the next section.

Tensor Diagrams. Following the convention in quantum physics (Cichocki et al., 2016), we introduce *tensor diagrams* in Figure 1, graphical representations of multi-dimensional arrays. In these diagrams, an array is represented as a *vertex (node)*, whose *order* is denoted by the number of *edges (links)* connected to the node, where each edge corresponding to a *mode (axis)*. The *dimension* of a mode is denoted by a number with the corresponding edge.

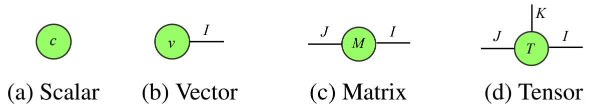

(a) Scalar (b) Vector (c) Matrix (d) Tensor

Figure 1. Tensor diagrams of a scalar $c \in \mathbb{R}$, a vector $v \in \mathbb{R}^I$, a matrix $M \in \mathbb{R}^{I \times J}$ and a third-order tensor $\mathcal{T} \in \mathbb{R}^{I \times J \times K}$.

Tensor Operations. With these diagrams, we can represent the operations between (higher-order) tensors graphically. In Figure 2, we illustrate three *tensor operations* commonly used in neural networks, namely *tensor contraction*, *tensor convolution* and *batch product*. In these figures, an operation is denoted by connecting the edges from both input tensors, where the type of operation is distinguished by the shape/color of the edges: solid line stands for tensor contraction or batch product, and dotted line represents tensor convolution. Notice that a tensor operation can be arbitrarily complicated by linking multiple edges from multiple tensors simultaneously, see Figure 4 for an example.

4. Tensor-Trains and Sequence Modeling

The goal of tensor decomposition is to represent a higher-order tensor in a set of smaller and lower-order *core tensors*, with fewer parameters while preserving essential information. Yu et al. (2017) used *tensor-train decomposition* (Oseledets, 2011) to reduce both parameters and computations in higher-order recurrent model. We will review the standard model in the first part of this section.

However, the approach by Yu et al. (2017) only considers recurrent models with vector inputs. Since spatial structure is not preserved by standard tensor-train decomposition, their approach cannot be tensor-train cannot be extended to cope with video/image inputs directly. In the second part, we propose a novel *Convolutional Tensor-Train Decomposition* (CTTD). With CTTD, a large convolutional kernel is factorized into a chain of smaller kernels. We show that such decomposition can significantly reduce both parameters and operations of higher-order spatio-temporal recurrent models.

Throughout this section, We will use tensor diagrams to illustrate the operations in all models. The exact mathematical expression for these models are included in Appendix A.

Standard Tensor-Train Decomposition. Given an m-*order* tensor $\mathcal{T} \in \mathbb{R}^{I_1 \times \cdots \times I_m}$ with I_l as the *dimension* of its l-th *mode*, a standard tensor-train decomposition (TTD) factorizes the tensor $\mathcal{T}$ into a set of m *core tensors* $\{\mathcal{T}^l\}_{l=1}^m$ with $\mathcal{T}^l \in \mathbb{R}^{I_l \times R_l \times R_{l+1}}$, illustrated in Figure 3a. In TTD, the *ranks* $\{R_l\}_{l=1}^{m-1}$ control the number of parameters in the *tensor-train format*, and the original tensor $\mathcal{T}$ of size $(\prod_{l=1}^m I_l)$ is compressed to $(\sum_{l=1}^m I_l R_{l-1} R_l)$, i.e. the complexity of TTD only grows linearly with the order m (assuming R_l's are constants). Therefore, TTD is commonly used to approximate higher-order tensors with fewer parameters.

As shown in Figure 3a, the tensor diagram for TTD takes a "train" shape (and therefore its name). The sequential structure in TTD makes it particularly suitable for sequence modeling. Consider a higher-order model that predicts a scalar output $y \in \mathbb{R}$ based on the outer product of a sequence of input vectors $\{\boldsymbol{x}^l\}_{l=1}^m$ with $\boldsymbol{x}^l \in \mathbb{R}^{I_l}$,

$$y = \left\langle \mathcal{T}, \left(\boldsymbol{x}^1 \otimes \boldsymbol{x}^2 \cdots \otimes \boldsymbol{x}^m\right) \right\rangle \quad (1)$$

This model is intractable in practice since the number of parameters in $\mathcal{T} \in \mathbb{R}^{I_1 \times \cdots I_m}$ (and therefore computational complexity) grows exponentially with the order m. Now suppose $\mathcal{T}$ takes a tensor-train format as in Figure 3a, Equation (1) can be efficiently evaluated sequentially from left to right as in Figure 3c: $\boldsymbol{x}^1$ first interacts with $\mathcal{T}^1$, and the intermediate result interacts with $\mathcal{T}^2$ and $\boldsymbol{x}^2$ simultaneously, and so on. Notice that the higher-order tensor $\mathcal{T}$ is never reconstructed in the process, therefore both space and computational complexities grow linearly (not exponentially as in Equation (1)) with the order m.

Convolutional Tensor-Train Decomposition. A convolutional layer (in neural networks) is typically parameterized by a tensor $\mathcal{T} \in \mathbb{R}^{K \times R_1 \times R_{m+1}}$, where K is the kernel size, and R_1, R_{m+1} are the number of input and output channels. Suppose the kernel size K takes the form $K = (\sum_{l=1}^m K_l) - m + 1$, we propose convolutional tensor-train decomposition (CTTD) that factorizes $\mathcal{T}$ into a set of m core tensors $\{\mathcal{T}^l\}_{l=1}^m$ with $\mathcal{T}^l \in \mathbb{R}^{K_l \times R_l \times R_{l-1}}$ as in Figure 3b, and denote $\mathcal{T} = \mathsf{CTTD}(\{\mathcal{T}^l\}_{l=1}^m)$. As in TTD, the *ranks* of CTTD $\{R_l\}_{l=1}^m$ control the complexity of the *convolutional tensor-train format*, and the number of parameters reduces from KR_1R_{m+1} to $\sum_{l=1}^m K_l R_l R_{l+1}$.

Similar to standard TTD, its convolutional counterpart can be used to compress higher-order spatio-temporal recurrent models with convolutional operations. Consider a model that predicts a feature $\mathcal{V} \in \mathbb{R}^{I'_m \times R_{m+1}}$ based on a sequence of input features $\{\mathcal{U}^l\}_{l=1}^m$ with $\mathcal{U}^l \in \mathbb{R}^{I_l \times R_l}$ (where I_l is

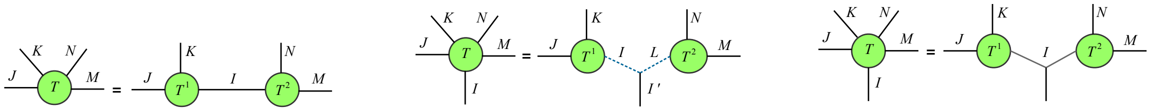

(a) Tensor contraction. $\mathcal{T}_{j,k,m,n} = \sum_i \mathcal{T}^1_{i,j,k}\, \mathcal{T}^2_{i,m,n}$

(b) Tensor convolution. $\mathcal{T}_{:,j,k,m,n} = \mathcal{T}^1_{:,j,k} * \mathcal{T}^2_{:,m,n}$

(c) Batch product. $\mathcal{T}_{i,j,k} = \mathcal{T}^2_{i,j,k} \mathcal{T}^2_{i,m,n}$

Figure 2. Diagrams of tensor operations. For all examples, the inputs are two third-order tensors $\mathcal{T}^1 \in \mathbb{R}^{I \times J \times K}$ and $\mathcal{T}^2 \in \mathbb{R}^{I \times M \times N}$, and the operations are on mode I. **(a)** In tensor contraction, the edges for operation must share the same dimension, and will vanish after contraction; **(b)** In tensor convolution, a new edge will emerge after the operation. Different from contraction, the dimensions for the operating edges may be different depending on the type of convolution. **(c)** In batch product, a new edge will also emerge after the operation. Different from convolution, the dimensions for all operating edges must be the same.

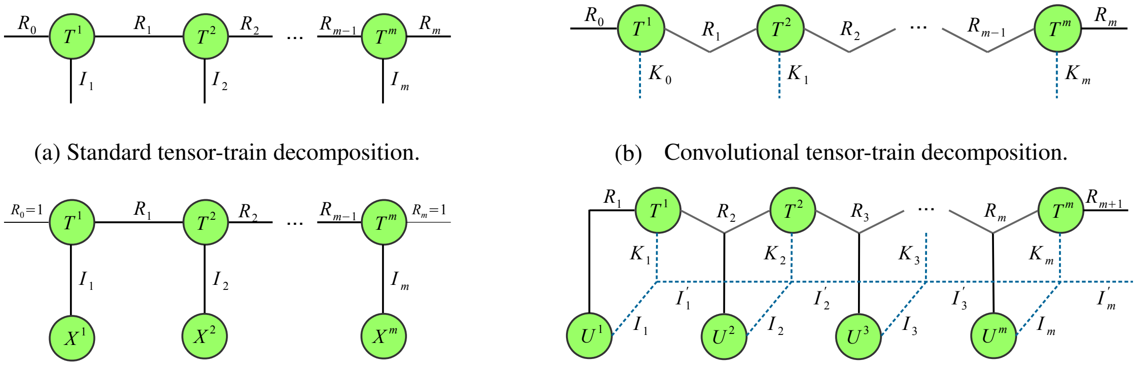

(a) Standard tensor-train decomposition.

(b) Convolutional tensor-train decomposition.

(c) Standard tensor-train for sequence modeling.

(d) Convolutional tensor-train for spatial-temporal modeling.

Figure 3. **(1)** In the first row, we illustrate the tensor diagrams for both standard tensor-train decomposition and convolutional tensor-train decomposition. Notice that convolutional TTD is different from the standard TTD in that it replaces dangling edges $\{I_l\}_{l=1}^m$ for contraction by ones $\{K_l\}_{l=1}^m$ for convolution. **(2)** In the second row, we illustrate the applications of both tensor-train decompositions in sequence modeling. (c) In standard TTD, all edges $\{I_1\}_{l=1}^m$ and $\{R_l\}_{l=1}^{m-1}$ are contracted. (d) In convolutional TTD, the edges $\{I_l\}_{l=1}^m$ are contracted, and edges $\{I_l\}_{l=1}^m$ and $\{K_l\}_{l=1}^m$ are involved in convolutions. Notice that in convolutional TTD, the edges $\{R_l\}_{l=1}^m$ for contraction is not directly linked to any vertex in order to avoid an extra dimension in $\mathcal{T}^l$. Both models can be evaluated by interacting the tensors from left to right to obtain the final output and take Figure 3d for an example: $\mathcal{U}^1$ is first interacted with $\mathcal{T}^1$, and the resulted tensor is further interacted with $\mathcal{T}^2$ and $\mathcal{U}^2$. The process repeats until all tensors are merged into one.

the feature length, and R_l is the number of channels in $\mathcal{U}^l$),

$$\mathcal{V}_{:,:,r_{m+1}} = \sum_{l=1}^{m} \mathcal{W}^l_{:,:,r_l,r_{m+1}} * \mathcal{U}^l_{:,:,r_l} \quad \text{with } \mathcal{W}^l = \mathsf{CTTD}\left(\{\mathcal{T}^k\}_{k=l}^m\right) \tag{2}$$

where $\mathcal{W}^l$ is the corresponding weights tensor for $\mathcal{U}^l$, which itself takes takes a convolutional tensor-train format in Figure 3b. The structure also admits an efficient algorithm: $\mathcal{U}^1$ is first interacted with $\mathcal{T}^1$, and the result is further interacted with $\mathcal{T}^2$ and $\mathcal{U}^2$ simultaneously. The process is illustrated in Figure 3d. Again, the original weights $\mathcal{W}^l$'s are never reconstructed in such a process. The overall operations of a third-order CTTD (Equation (2)) for two-dimensional features are illustrated in Figure 4a. In this paper, we denote Equation (2) simply as $\mathcal{V} = \mathsf{CTT}(\{\mathcal{T}^l\}_{l=1}^m, \{\mathcal{U}^l\}_{l=1}^m)$.

5. Convolutional Tensor-Train LSTM

Convolutional LSTM (ConvLSTM) is a basic building block for most recent video forecasting models (Xingjian et al., 2015), where the spatial information is encoded explicitly as tensors in the LSTM cells. In a ConvLSTM network, each cell is a first-order Markov model, where the hidden state is updated based on its previous step. In this section, we propose Convolutional Tensor-Train LSTM (Conv-TT-LSTM), where ConvLSTM is integrated with convolutional tensor-train to model higher-order spatio-temporal correlations explicitly. The proposed model is illustrated in Figure 4.

Notations. In this section, $*$ is overloaded to denote convolution between higher-order tensors. For instance, given a 4-th order weights tensor $\mathcal{W} \in \mathbb{R}^{K \times K \times S \times C}$ and a 3-rd order input tensor $\mathcal{X} \in \mathbb{R}^{H \times W \times S}$, $\mathcal{Y} = \mathcal{W} * \mathcal{X}$ computes a 3-rd output tensor $\mathcal{Y} \in \mathbb{R}^{H \times W \times T}$ as $\mathcal{Y}_{:,:,c} = \sum_{s=1} \mathcal{W}_{:,:,s,c} * \mathcal{X}_{:,:,s}$. The symbol $\circ$ is used to denote element-wise product between two tensors, and σ represents a function that performs

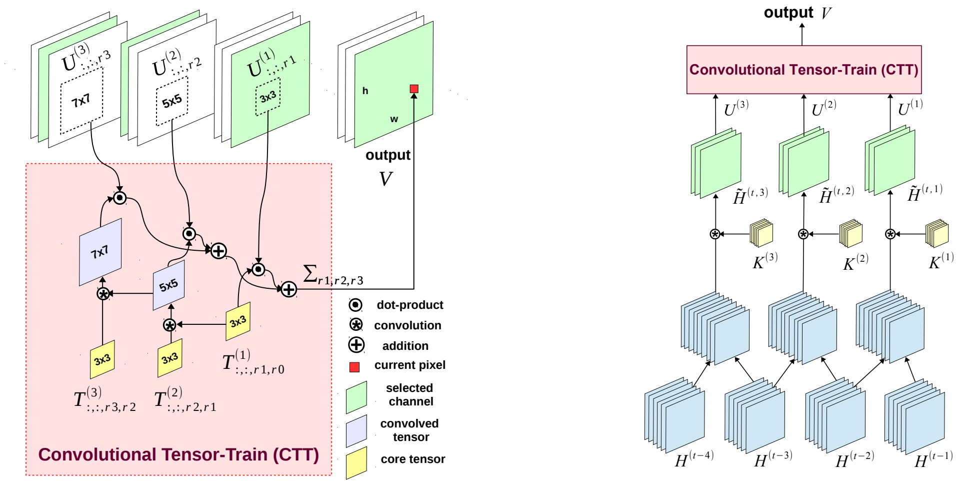

(a) Convolutional tensor-train decomposition.

(b) Convolutional tensor-train LSTM

Figure 4. Illustration of **(a) convolutional tensor-train decomposition** (Equation (2)) and **(b) convolutional tensor-train LSTM** (Equation (6)). The original frames to Conv-TT-LSTM are first grouped by a sliding window before fed into the convolutional tensor-train. In Conv-TT-LSTM, the CTTD is used with two minor modifications: (1) The edges for convolutions are extended to two-dimensional, i.e. I_l and K_l in Figure 3d are tuples of two dimensions $I_l = (H, W)$ and $K_l = (k, k)$; (2) The indices are named reversely such that they reflect the number of steps from the current output, e.g. $U^{(3)} = U^1$ and $U^{(1)} = U^3$ in Figure 3d.

element-wise (nonlinear) transformation on a tensor.

Convolutional Long Short-Term Memory (ConvLSTM). Xingjian et al. (2015) extended fully-connected LSTM to Convolutional LSTM to model spatio-temporal structures within each recurrent unit, where all features are encoded as third-order tensors with dimensions (height H × width W × channels C) and operations are replaced by convolutions between tensors. In each cell, the parameters are characterized by two 4-th order tensors $\mathcal{W} \in \mathbb{R}^{K \times K \times S \times 4C}$ and $\mathcal{T} \in \mathbb{R}^{K \times K \times C \times 4C}$, where K is the kernel size for convolutions, S, C are the numbers of channels of the inputs $\mathcal{X}^{(t)} \in \mathbb{R}^{H \times W \times S}$ and hidden states $\mathcal{H}^{(t)} \in \mathbb{R}^{H \times W \times C}$. At each time step t, a cell updates its hidden states $\mathcal{H}^{(t)}$ based on the previous step $\mathcal{H}^{(t-1)}$ and the current input $\mathcal{X}^{(t)}$.

$$[\mathcal{I}^{(t)}; \mathcal{F}^{(t)}; \tilde{\mathcal{C}}^{(t)}; \mathcal{O}^{(t)}] = \sigma(\mathcal{W} * \mathcal{X}^{(t)} + \mathcal{T} * \mathcal{H}^{(t-1)}) \quad (3)$$

$$\mathcal{C}^{(t)} = \tilde{\mathcal{C}}^{(t)} \circ \mathcal{I}^{(t)}; \quad \mathcal{H}^{(t)} = \mathcal{O}^{(t)} \circ \mathcal{C}^{(t)} \quad (4)$$

where $\sigma(\cdot)$ applies sigmoid on the input gate $\mathcal{I}^{(t)}$, forget gate $\mathcal{F}^{(t)}$, output gate $\mathcal{O}^{(t)}$, and $\tanh(\cdot)$ on memory cell $\tilde{\mathcal{C}}^{(t)}$. Notice that $\mathcal{C}^{(t)}$, $\mathcal{I}^{(t)}$, $\mathcal{F}^{(t)}$, $\mathcal{O}^{(t)} \in \mathbb{R}^{H \times W \times C}$ are all 3-rd order tensors.

Convolutional Tensor-Train LSTM (Conv-TT-LSTM). We introduce a higher-order recurrent unit to capture multi-steps spatio-temporal correlations in ConvLSTM, where the hidden state $\mathcal{H}^{(t)}$ is updated based on its n previous steps $\{\mathcal{H}^{(t-l)}\}_{l=1}^{n}$ with an m-order CTT as in Equation 2. Concretely, suppose the parameters in CTT are characterized by m tensors of 4-th order $\{\mathcal{T}^{(o)}\}_{o=1}^{m}$, Conv-TT-LSTM replaces Equation (3) in ConvLSTM by two equations:

$$\tilde{\mathcal{H}}^{(t,o)} = f\left(\mathcal{K}^{(o)}, \{\mathcal{H}^{(t-l)}\}_{l=1}^{n}\right), \forall o \in [m] \quad (5)$$

$$\begin{aligned}\left[\mathcal{I}^{(t)}; \mathcal{F}^{(t)}; \tilde{\mathcal{C}}^{(t)}; \mathcal{O}^{(t)}\right] = \sigma\big(&\mathcal{W} * \mathcal{X}^{(t)} + \\ &\mathsf{CTT}\big(\{\mathcal{T}^{(o)}\}_{o=1}^{m}, \{\tilde{\mathcal{H}}^{(t,o)}\}_{o=1}^{m}\big)\big)\end{aligned} \quad (6)$$

(1) Since $\mathsf{CCT}(\{\mathcal{T}^{(l)}\}_{l=1}^{m}, \cdot)$ takes a series of m tensors as inputs, the first step in (5) maps the n inputs $\{\mathcal{H}^{(t-l)}\}_{l=1}^{n}$ to m intermediate tensors $\{\mathcal{H}^{(t,o)}\}_{o=1}^{m}$ with a function f. **(2)** These m tensors $\{\tilde{\mathcal{H}}^{(t,o)}\}_{o=1}^{m}$ are then fed into $\mathsf{CCT}(\{\mathcal{T}^{(l)}\}_{l=1}^{m}, \cdot)$ and compute the gates per Equation (6).

In this work, we devise a *sliding window* strategy to compute Equation (5). With this strategy, a sliding subset of $\{\mathcal{H}^{(l)}\}$ are concatenated into $\hat{\mathcal{H}}^{(t,o)}$, which is then transformed into an input $\tilde{\mathcal{H}}^{(t,o)}$ to the convolutional tensor-train (See Figure 4b). Concretely, the Conv-TT-LSTM model computes each $\tilde{\mathcal{H}}^{(t,o)}$ by the following equation:

$$\begin{aligned}\tilde{\mathcal{H}}^{(t,o)} &= \mathcal{K}^{(o)} * \hat{\mathcal{H}}^{(t,o)} \\ &= \mathcal{K}^{(o)} * \left[\mathcal{H}^{(t-n+m-l)}; \cdots \mathcal{H}^{(t-l)}\right]\end{aligned} \quad (7)$$

The n previous states $\{\mathcal{H}^{(l)}\}_{l=1}^{n}$ are first concatenated (over time axis) into m tensors $\{\hat{\mathcal{H}}^{(t,o)}\}_{o=1}^{m}$ by a sliding window, each of which has size $\hat{\mathcal{H}}^{(t,o)} \in \mathbb{R}^{H \times W \times D \times C}$ (with $D = n - m + 1$) and thereafter mapped to $\tilde{\mathcal{H}}^{(t,o)} \in \mathbb{R}^{H \times W \times R}$ by 3D-convolution with a kernel $\mathcal{K}^{(l)} \in \mathbb{R}^{k \times k \times D \times R}$.

We note that a *fixing window* strategy is also feasible here, where all $\mathcal{U}l$'s are concatenated into a single tensor, which repeatedly used in every single input. The discussion of fixed window and the empirical comparison against sliding window are shown in Appendix B.

6. Experiments

We first evaluate our approach on the synthetic Moving-MNIST-2 dataset (Srivastava et al., 2015). In addition, we use KTH human action dataset (Laptev et al., 2004) to test the performance of our proposed models in more realistic scenario.

Model Architecture. All experiments use a stack of 12-layers of ConvLSTM or Conv-TT-LSTM with 32 channels for the first and last 3 layers, and 48 channels for the 6 layers in the middle. A convolutional layer is applied on top of all recurrent layers to compute the predicted frames, followed by an extra sigmoid layer for colored videos. Following Byeon et al. (2018), two skip connections performing concatenation over channels are added between (3, 9) and (6, 12) layers. Illustration of the network architecture is included in Appendix D.All parameters are initialized by Xavier's normalized initializer (Glorot & Bengio, 2010) and initial states in ConvLSTM or Conv-TT-LSTM are initialized as zeros.

Evaluation Metrics. We use two traditional metrics MSE (or PSNR) and SSIM (Wang et al., 2004), and a recently proposed deep-learning based metric LPIPS (Zhang et al., 2018), which measures the similarity between deep features. Since MSE (or PSNR) is based on pixel-wise difference, it favors vague and blurry predictions, which is not a proper measurement of perceptual similarity. While SSIM was originally proposed to address the problem, Zhang et al. (2018) shows that their proposed LPIPS metric aligns better to human perception.

Learning Strategy. All models are trained with ADAM optimizer (Kingma & Ba, 2014) with $\mathcal{L}_1 + \mathcal{L}_2$ loss. Learning rate decay and scheduled sampling (Bengio et al., 2015) are used to ease training. Scheduled sampling is started once the model does not improve in 20 epochs (in term of validation loss), and the sampling ratio is decreased linearly from 1 until it reaches zero (by 2×10^{-4} each epoch for Moving-MNIST-2 and 5×10^{-4} for KTH). Learning rate decay is further activated if the loss does not drop in 20 epochs, and the rate is decreased exponentially by 0.98 every 5 epochs.

Hyper-parameters Selection. We perform a wide range of hyper-parameters search for Conv-TT-LSTM to identify the best model. The full list of search values are summarized in Table 4 (Appendix C).The initial learning rate of 10^{-3} is found for baseline ConvLSTM and 10^{-4} for our proposed Conv-TT-LSTM. We found that the Conv-TT-LSTM models suffer from exploding gradients when learning rate is high, therefore we also explore various gradient clipping values and select 1 for all models. All other hyper-parameters are selected using the best validation performance.

6.1. Moving-MNIST-2 Dataset

The Moving-MNIST-2 dataset is generated by moving two digits of size 28×28 in MNIST dataset within a 64×64 black canvas. These digits are placed at a random initial location, and move with constant velocity in the canvas and bounce when they reach the boundary. Following Wang et al. (2018a), we generate 10,000 videos for training, 3,000 for validation, and 5,000 for test with default parameters in the generator[5]. All our models are trained to predict 10 frames given 10 input frames.

Multi-Steps Prediction. Table 1 reports the average statistics for 10 and 30 frames prediction, and Figure 5 shows comparison of per-frame statistics for PredRNN++ model, ConvLSTM baseline and our proposed Conv-TT-LSTM model. **(1)** Our Conv-TT-LSTM model consistently outperform the 12-layer ConvLSTM baseline for both 10 and 30 frames prediction *with fewer parameters*; **(2)** The Conv-TT-LSTM outperform previous approaches in terms of SSIM and LPIPS (especially on 30 frames prediction), *with less than one fifth of the model parameters*.

We reproduce the PredRNN++ model (Wang et al., 2018a) from their source code[2], and we find that **(1)** The PredRNN++ model tends to output vague and blurry results in long-term prediction (especially after 20 steps). **(2)** and our Conv-TT-LSTMs are able to produce sharp and realistic digits over all steps. An example of comparison for different models is shown in Figure 6. The visualization is consistent with the results in Table 1 and Figure 5.

Ablation Studies on CTTD The core component in our Conv-TT-LSTM is a higher-order convolutional TTD. In the following ablation studies, we present the necessity of (1) higher-order model and (2) convolutional operations in the decomposition for capturing long-term spatio-temporal information. We compare the performance of two ablated models against our Conv-TT-LSTM in Table 3. The single

[1] The results are cited from the original paper (Wang et al., 2018a), where the miscalculation of MSE is corrected in the table.

[2] The results for PredRNN++ are reproduced from https://github.com/Yunbo426/predrnn-pp with the same datasets in this paper. The original implementation crops each frame into patches as the input to the model. We find such preprocessing is unnecessary and the performance of reproduced model is better than the one in the original paper.

[3] The results for E3D-LSTM are cited from the original paper (Wang et al., 2018b).

[4] The results are reproduced with the pretrained model by the authors https://github.com/google/e3d_lstm.

[5] The Python code for Moving-MNIST-2 generator is publicly available online in https://github.com/jthsieh/DDPAE-video-prediction/blob/master/data/moving_mnist.py.

Table 1. Comparison of 10 and 30 frames prediction on Moving-MNIST-2 test set, where lower MSE values (in 10^{-3}) / higher SSIM / lower LPIPS values (in 10^{-3}) indicate better results. The reported Conv-TT-LSTM model is with order 3, steps 3, and ranks 8.

Method	(10 -> 10)			(10 -> 30)			# params.
	MSE	SSIM	LPIPS	MSE	SSIM	LPIPS	
ConvLSTM (Xingjian et al., 2015)	25.22	0.713	-	38.13	0.595	-	7.58M
CDNA (Finn et al., 2016)	23.78	0.728	-	34.74	0.609	-	-
VPN (Kalchbrenner et al., 2017)	15.65	0.870	-	31.64	0.620	-	-
PredRNN++ (Wang et al., 2018a) (original) [1]	11.35	0.898	-	22.24	0.814	-	15.05M
PredRNN++ (Wang et al., 2018a) (retrained) [2]	10.29	0.913	59.51	**20.53**	0.834	139.9	
E3D-LSTM (Wang et al., 2018b) (original) [3]	**10.08**	0.910	-	-	-	-	41.94M
E3D-LSTM (Wang et al., 2018b) (pretrained) [4]	20.23	0.869	76.12	32.37	0.803	150.3	
ConvLSTM (baseline)	18.17	0.882	67.13	33.08	0.806	140.1	3.97M
Conv-TT-LSTM (ours)	12.96	**0.915**	**40.54**	25.81	**0.840**	**90.38**	2.69M

Table 2. Evaluation of multi-steps prediction on KTH dataset, where higher PSNR/SSIM values and lower LPIPS values indicate better predictive results. The reported Conv-TT-LSTM model here is with order 3, steps 3, and ranks 8. Our Conv-TT-LSTM outperforms ConvLSTM baseline and all previous approach in terms of SSIM and LPIPS.

Method	(10 -> 20)			(10 -> 40)			# Parameters
	PSNR	SSIM	LPIPS	PSNR	SSIM	LPIPS	
ConvLSTM (Xingjian et al., 2015)	23.58	0.712	-	22.85	0.639	-	7.58M
MCNET (Villegas et al., 2017)	25.95	0.804	-	-	-	-	-
PredRNN++ (Wang et al., 2018a) (original)[1]	28.46	0.865	-	25.21	0.741	-	15.05M
PredRNN++ (Wang et al., 2018a) (retrained)[2]	28.62	0.888	228.9	26.94	0.865	279.0	
E3D-LSTM (Wang et al., 2018b) (original)[3]	**29.31**	0.879	-	**27.24**	0.810	-	41.94M
E3D-LSTM (Wang et al., 2018b) (pretrained)[4]	27.92	0.893	298.4	26.55	0.878	328.8	
ConvLSTM (baseline)	28.21	0.903	137.1	26.01	0.876	201.3	3.97M
Conv-TT-LSTM (ours)	28.36	**0.907**	**133.4**	26.11	**0.882**	**191.2**	**2.69M**

Table 3. Ablation studies of higher-order Conv-TT-LSTM model. In these experiments, we evaluate the necessity of (1) higher-order model and (2) convolutional operations in the decomposition. The experimental results show that the ablated Conv-TT-LSTMs have similar performance to the ConvLSTM baseline.

Conv-TT-LSTM	(10 -> 30)			# parameters
	MSE($\times 10^{-3}$)	SSIM	LPIPS	
CTTD with 1×1 filters (similar to standard TTD)				
single order	31.52	0.810	148.7	2.36M
order 3	34.84	0.800	151.2	2.37M
CTTD with 5×5 filters				
single order	33.08	0.806	140.1	3.97M
order 3	**28.88**	**0.831**	**104.1**	2.65M

order means that the higher-order model is replaced to a first-order model (Tensor order=1). By replacing 3×3 filters to 1×1 in CTTD, the effect of convolutions in CTTD is demonstrated compared to the standard TTD. The results show that the ablated models at best achieve similar performance of ConvLSTM baseline, which shows both higher-order model and convolutional operations are necessary for long-term video prediction.

6.2. KTH Action Dataset

KTH action dataset (Laptev et al., 2004) contains videos of 25 individuals performing 6 types of actions on a simple background. Our experimental setup follows Wang et al. (2018a), which uses persons 1-16 for training and 17-25 for testing, and each frame is resized to 128×128 pixels. All our models are trained to predict 10 frames given 10 input frames. During training, we randomly select 20 contiguous frames from the training videos as a sample and group every 10,000 samples into one epoch to apply the learning strategy as explained at the beginning of this section.

Results. In Table 2, we report the evaluation on both 20 and 40 frames prediction. **(1)** Our models are consistently better than the ConvLSTM baseline for both 20 and 40 frames prediction. **(2)** While our proposed Conv-TT-LSTMs achieve lower SSIM value compared to the state-of-the-art models in 20 frames prediction, they outperform all previous models in LPIPS for both 20 and 40 frames prediction. An example of the predictions by the baseline and Conv-TT-LSTMs is shown in Figure 6.

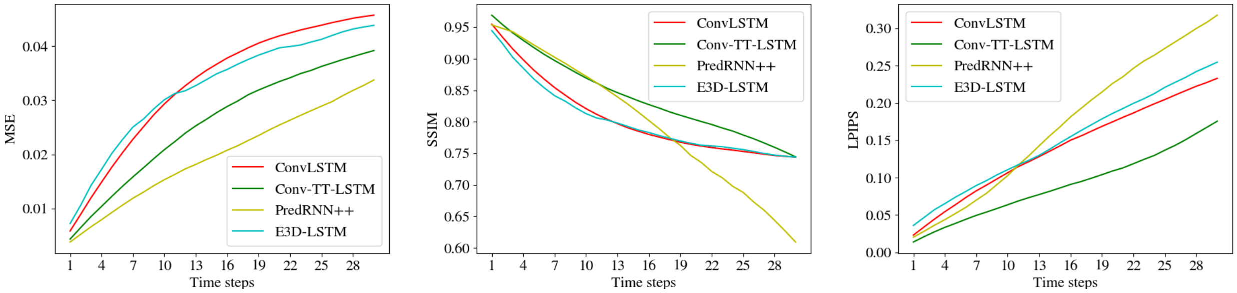

Figure 5. Frame-wise comparison in MSE, SSIM and PIPS on Moving-MNIST-2 dataset. For MSE and LPIPS, lower curves denote higher quality; while for SSIM, higher curves imply better quality. Our Conv-TT-LSTM performs better than ConvLSTM baseline, PredRNN++ (Wang et al., 2018a) and E3D-LSTM (Wang et al., 2018b) in all metrics (except for PredRNN++ in term of MSE).

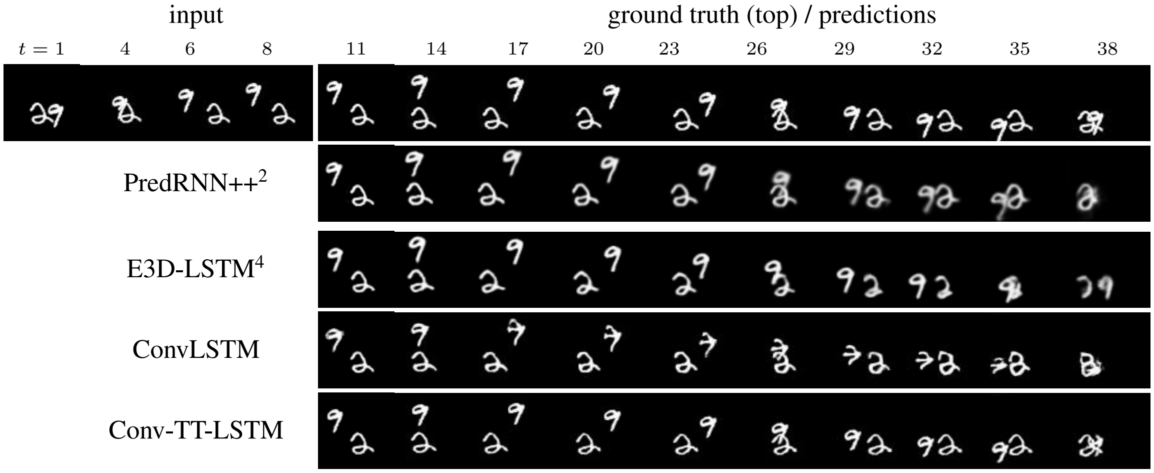

Figure 6. 30 frames prediction on Moving-MNIST given 10 input frames. Every 3 frames are shown. The first frames ($t = 1$ and 11) are animations. To view the animation, Adobe reader is required.

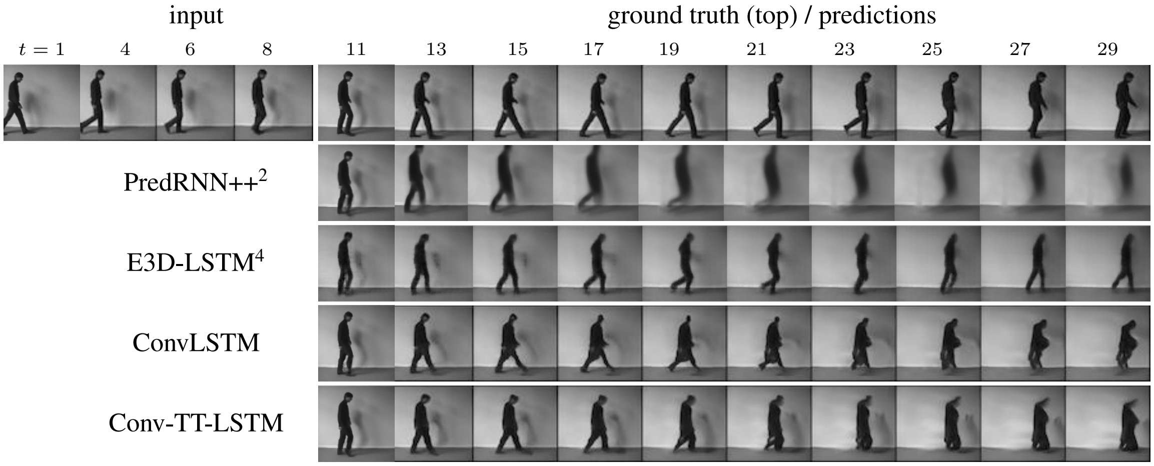

Figure 7. 20 frames prediction on KTH given 10 input frames. Every 2 frames are shown. The first frames ($t = 1$ and 11) are animations. To view the animation, Adobe reader is required.

7. Conclusion

In this paper, we proposed *Convolutional Tensor-Train Decomposition* (CTTD) to factorize a large convolutional kernel into a set of smaller *core tensors*. We applied CTTD to efficiently construct *convolutional tensor-train LSTM* (Conv-TT-LSTM), a higher-order recurrent neural network, that is capable to effectively capture long-term spatio-temporal correlations. We demonstrated the capacity of our proposed Conv-TT-LSTM on video prediction, and showed our model outperforms standard ConvLSTM and produce better results compared to other state-of-the-art models with fewer parameters. Utilizing the proposed model for high-resolution videos is still challenging due to gradient vanishing or explosion. Future direction will include investigating other training strategies or model designs to ease the training.

References

Alahi, A., Goel, K., Ramanathan, V., Robicquet, A., Fei-Fei, L., and Savarese, S. Social lstm: Human trajectory prediction in crowded spaces. In *Proceedings of the IEEE conference on computer vision and pattern recognition*, pp. 961–971, 2016.

Anandkumar, A., Ge, R., Hsu, D., Kakade, S. M., and Telgarsky, M. Tensor decompositions for learning latent variable models. *The Journal of Machine Learning Research*, 15(1):2773–2832, 2014.

Babaeizadeh, M., Finn, C., Erhan, D., Campbell, R. H., and Levine, S. Stochastic variational video prediction. *arXiv preprint arXiv:1710.11252*, 2017.

Bengio, S., Vinyals, O., Jaitly, N., and Shazeer, N. Scheduled sampling for sequence prediction with recurrent neural networks. In *Advances in Neural Information Processing Systems*, pp. 1171–1179, 2015.

Byeon, W., Wang, Q., Kumar Srivastava, R., and Koumoutsakos, P. Contextvp: Fully context-aware video prediction. In *Proceedings of the European Conference on Computer Vision (ECCV)*, pp. 753–769, 2018.

Cichocki, A., Lee, N., Oseledets, I., Phan, A.-H., Zhao, Q., Mandic, D. P., et al. Tensor networks for dimensionality reduction and large-scale optimization: Part 1 low-rank tensor decompositions. *Foundations and Trends® in Machine Learning*, 9(4-5):249–429, 2016.

Denton, E. and Fergus, R. Stochastic video generation with a learned prior. In *35th International Conference on Machine Learning, ICML 2018*, pp. 1906–1919. International Machine Learning Society (IMLS), 2018.

Denton, E. L. et al. Unsupervised learning of disentangled representations from video. In *Advances in neural information processing systems*, pp. 4414–4423, 2017.

Finn, C. and Levine, S. Deep visual foresight for planning robot motion. In *2017 IEEE International Conference on Robotics and Automation (ICRA)*, pp. 2786–2793. IEEE, 2017.

Finn, C., Goodfellow, I., and Levine, S. Unsupervised learning for physical interaction through video prediction. In *Advances in neural information processing systems*, pp. 64–72, 2016.

Glorot, X. and Bengio, Y. Understanding the difficulty of training deep feedforward neural networks. In *Proceedings of the thirteenth international conference on artificial intelligence and statistics*, pp. 249–256, 2010.

Hochreiter, S. and Schmidhuber, J. Long short-term memory. *Neural computation*, 9(8):1735–1780, 1997.

Hsieh, J.-T., Liu, B., Huang, D.-A., Fei-Fei, L. F., and Niebles, J. C. Learning to decompose and disentangle representations for video prediction. In *Advances in Neural Information Processing Systems*, pp. 517–526, 2018.

Kalchbrenner, N., van den Oord, A., Simonyan, K., Danihelka, I., Vinyals, O., Graves, A., and Kavukcuoglu, K. Video pixel networks. In *Proceedings of the 34th International Conference on Machine Learning-Volume 70*, pp. 1771–1779. JMLR. org, 2017.

Kim, Y.-D., Park, E., Yoo, S., Choi, T., Yang, L., and Shin, D. Compression of deep convolutional neural networks for fast and low power mobile applications. *arXiv preprint arXiv:1511.06530*, 2015.

Kingma, D. P. and Ba, J. Adam: A method for stochastic optimization. *arXiv preprint arXiv:1412.6980*, 2014.

Kolbeinsson, A., Kossaifi, J., Panagakis, Y., Anandkumar, A., Tzoulaki, I., and Matthews, P. Stochastically rank-regularized tensor regression networks. *arXiv preprint arXiv:1902.10758*, 2019.

Kolda, T. G. and Bader, B. W. Tensor decompositions and applications. *SIAM review*, 51(3):455–500, 2009.

Kossaifi, J., Lipton, Z., Khanna, A., Furlanello, T., and Anandkumar, A. Tensor regression networks. *arXiv*, 2017.

Kossaifi, J., Bulat, A., Panagakis, Y., and Pantic, M. Efficient n-dimensional convolutions via higher-order factorization. *arXiv preprint arXiv:1906.06196*, 2019.

Laptev, I., Caputo, B., et al. Recognizing human actions: a local svm approach. In *null*, pp. 32–36. IEEE, 2004.

Lebedev, V., Ganin, Y., Rakhuba, M., Oseledets, I., and Lempitsky, V. Speeding-up convolutional neural networks using fine-tuned cp-decomposition. *arXiv preprint arXiv:1412.6553*, 2014.

Lee, A. X., Zhang, R., Ebert, F., Abbeel, P., Finn, C., and Levine, S. Stochastic adversarial video prediction. *arXiv preprint arXiv:1804.01523*, 2018.

Lotter, W., Kreiman, G., and Cox, D. Deep predictive coding networks for video prediction and unsupervised learning. *arXiv preprint arXiv:1605.08104*, 2016.

Ma, X., Zhang, P., Zhang, S., Duan, N., Hou, Y., Song, D., and Zhou, M. A tensorized transformer for language modeling. *arXiv preprint arXiv:1906.09777*, 2019.

Mathieu, M., Couprie, C., and LeCun, Y. Deep multi-scale video prediction beyond mean square error. *arXiv preprint arXiv:1511.05440*, 2015.

Novikov, A., Podoprikhin, D., Osokin, A., and Vetrov, D. P. Tensorizing neural networks. In *Advances in neural information processing systems*, pp. 442–450, 2015.

Oseledets, I. V. Tensor-train decomposition. *SIAM Journal on Scientific Computing*, 33(5):2295–2317, 2011.

Soltani, R. and Jiang, H. Higher order recurrent neural networks. *arXiv preprint arXiv:1605.00064*, 2016.

Srivastava, N., Mansimov, E., and Salakhudinov, R. Unsupervised learning of video representations using lstms. In *International conference on machine learning*, pp. 843–852, 2015.

Su, J., Li, J., Bhattacharjee, B., and Huang, F. Tensorized spectrum preserving compression for neural networks. *arXiv preprint arXiv:1805.10352*, 2018.

Sutskever, I., Martens, J., and Hinton, G. E. Generating text with recurrent neural networks. In *Proceedings of the 28th International Conference on Machine Learning (ICML-11)*, pp. 1017–1024, 2011.

Tjandra, A., Sakti, S., and Nakamura, S. Compressing recurrent neural network with tensor train. In *2017 International Joint Conference on Neural Networks (IJCNN)*, pp. 4451–4458. IEEE, 2017.

Vaswani, A., Shazeer, N., Parmar, N., Uszkoreit, J., Jones, L., Gomez, A. N., Kaiser, Ł., and Polosukhin, I. Attention is all you need. In *Advances in neural information processing systems*, pp. 5998–6008, 2017.

Villegas, R., Yang, J., Hong, S., Lin, X., and Lee, H. Decomposing motion and content for natural video sequence prediction. *arXiv preprint arXiv:1706.08033*, 2017.

Wang, Y., Long, M., Wang, J., Gao, Z., and Philip, S. Y. Predrnn: Recurrent neural networks for predictive learning using spatiotemporal lstms. In *Advances in Neural Information Processing Systems*, pp. 879–888, 2017.

Wang, Y., Gao, Z., Long, M., Wang, J., and Yu, P. S. Predrnn++: Towards a resolution of the deep-in-time dilemma in spatiotemporal predictive learning. *arXiv preprint arXiv:1804.06300*, 2018a.

Wang, Y., Jiang, L., Yang, M.-H., Li, L.-J., Long, M., and Fei-Fei, L. Eidetic 3d lstm: A model for video prediction and beyond. *preprint*, 2018b.

Wang, Z., Bovik, A. C., Sheikh, H. R., Simoncelli, E. P., et al. Image quality assessment: from error visibility to structural similarity. *IEEE transactions on image processing*, 13(4):600–612, 2004.

Weissenborn, D., Täckström, O., and Uszkoreit, J. Scaling autoregressive video models. *arXiv preprint arXiv:1906.02634*, 2019.

Xingjian, S., Chen, Z., Wang, H., Yeung, D.-Y., Wong, W.-K., and Woo, W.-c. Convolutional lstm network: A machine learning approach for precipitation nowcasting. In *Advances in neural information processing systems*, pp. 802–810, 2015.

Yang, Y., Krompass, D., and Tresp, V. Tensor-train recurrent neural networks for video classification. In *Proceedings of the 34th International Conference on Machine Learning-Volume 70*, pp. 3891–3900. JMLR. org, 2017.

Yu, R., Zheng, S., Anandkumar, A., and Yue, Y. Long-term forecasting using tensor-train rnns. *arXiv preprint arXiv:1711.00073*, 2017.

Zhang, R., Isola, P., Efros, A. A., Shechtman, E., and Wang, O. The unreasonable effectiveness of deep features as a perceptual metric. In *Proceedings of the IEEE Conference on Computer Vision and Pattern Recognition*, pp. 586–595, 2018.

Zhang, S., Wu, Y., Che, T., Lin, Z., Memisevic, R., Salakhutdinov, R. R., and Bengio, Y. Architectural complexity measures of recurrent neural networks. In *Advances in neural information processing systems*, pp. 1822–1830, 2016.

Appendix: Convolutional Tensor-Train LSTM for Spatio-temporal Learning

A. Mathematical Expressions for Tensor-Trains

In Section 4, we introduced the concepts of standard and convolutional tensor-trains and their applications in sequence modeling in *tensor diagrams*. In this section, we present their equivalent forms in *mathematical expressions*.

A.1. Standard Tensor-Train Decomposition and Temporal Modeling

Notice that tensor diagram of standard tensor-train in Figure 3a can be expressed as

$$\mathcal{T}_{i_1, \cdots, i_m} \triangleq \sum_{r_1 = 1}^{R_1} \cdots \sum_{r_{m-1} = 1}^{R_{m-1}} \mathcal{T}^1_{i_1, 1, r_1} \cdots \mathcal{T}^m_{i_m, r_{m-1}, 1} \tag{8}$$

and the higher-order regressive model in Equation 1 can be rewritten as

$$y = \sum_{i_1 = 1}^{I_1} \cdots \sum_{i_m = 1}^{I_m} \mathcal{T}_{i_1, \cdots, i_m} \, \boldsymbol{x}^1_{i_1} \, \cdots \, \boldsymbol{x}^m_{i_m} \tag{9}$$

Then the sequential algorithm illustrated in Figure 3c is equivalent to

$$\boldsymbol{v}^l_{r_l} = \sum_{i_l = 1}^{I_l} \sum_{r_{l-1} = 1}^{R_l} \mathcal{T}^l_{i_l, r_{l-1}, r_l} \, \boldsymbol{v}^{l-1}_{r_{l-1}} \, \boldsymbol{x}^l_{i_l} \tag{10}$$

where the vectors $\{\boldsymbol{v}^l\}_{l=1}^m$ (with $\boldsymbol{v}^l \in \mathbb{R}^{R_l}$) are intermediate steps, with initial input $\boldsymbol{v}^0 = 1$, and final output $y = \boldsymbol{v}^m$. We will prove the correctness of this algorithm by induction.

Proof of Equation 10 We denote the standard tensor-train decomposition in Equation 8 as $\mathcal{T} = \mathsf{TTD}(\{\mathcal{T}^l\}_{l=1}^m)$, then Equation 9 can be rewritten as Equation 11 since $R_0 = 1$ and $v^{(0)}_1 = 1$.

$$\begin{aligned}
v &= \sum_{r_0 = 1}^{R_0} \sum_{i_1 = 1}^{I_1} \cdots \sum_{i_m = 1}^{I_m} \mathsf{TTD}\left(\{\mathcal{T}^l\}_{l=1}^m\right)_{i_1, \cdots, i_m} \boldsymbol{v}^0_{r_0} \left(\boldsymbol{x}^1 \otimes \cdots \otimes \boldsymbol{x}^m\right)_{i_1, \cdots, i_m} && (11) \\
&= \sum_{r_0 = 1}^{R_0} \sum_{i_1 = 1}^{I_1} \cdots \sum_{i_m = 1}^{I_m} \left(\sum_{r_1 = 1}^{R_1} \cdots \sum_{r_{m-1} = 1}^{R_{m-1}} \mathcal{T}^1_{i_1, r_0, r_1} \cdots \mathcal{T}^m_{i_m, r_{m-1}, r_m} \right) \boldsymbol{v}^0_{r_0} \, \boldsymbol{x}^1_{i_1} \cdots \boldsymbol{x}^m_{i_m} && (12) \\
&= \sum_{r_1 = 1}^{R_1} \sum_{i_2 = 1}^{I_2} \cdots \sum_{i_m = 1}^{I_m} \left(\sum_{r_2 = 1}^{R_2} \cdots \sum_{r_{m-1} = 1}^{R_{m-1}} \mathcal{T}^2_{i_2, r_1, r_2} \cdots \mathcal{T}^m_{i_m, r_{m-1}, r_m} \right) \left(\sum_{r_0 = 1}^{R_0} \sum_{i_1 = 1}^{I_1} \mathcal{T}^1_{i_1, r_0, r_1} \, \boldsymbol{v}^0_{r_0} \, \boldsymbol{x}^1_{i_1} \right) \boldsymbol{u}^2_{i_2} \cdots \boldsymbol{x}^m_{i_m} && (13) \\
&= \sum_{r_1 = 1}^{R_1} \sum_{i_2 = 1}^{I_2} \cdots \sum_{i_m = 1}^{I_m} \mathsf{TTD}\big(\{\mathcal{T}^l\}_{l=2}^m\big)_{i_1, \cdots, i_m} \boldsymbol{v}^1_{r_1} \left(\boldsymbol{x}^2 \otimes \cdots \otimes \boldsymbol{x}^m\right)_{i_2, \cdots, i_m} && (14)
\end{aligned}$$

where $R_0 = 1$, $\boldsymbol{v}^0 1 = 1$ and the sequential algorithm in Equation 10 is performed at Equation 13.

A.2. Convolutional Tensor-Train Decomposition and Spatio-Temporal Modeling

Notice that the convolutional tensor-train in Figure 3b can be expressed as

$$\mathcal{T}_{:, r_1, r_{m+1}} \triangleq \sum_{r_2 = 1}^{R_2} \cdots \sum_{r_m = 1}^{R_m} \mathcal{T}^1_{:, r_1, r_2} * \cdots * \mathcal{T}^m_{:, r_m, r_{m+1}} \tag{15}$$

And the sequential algorithm illustrated in Figure 3d can be equivalently stated as

$$\mathcal{V}^{l+1}_{:, r_{l+1}} = \sum_{r_l = 1}^{R_l} \mathcal{T}^l_{:, r_l, r_{l+1}} * \left(\mathcal{V}^l_{:, r_l} + \mathcal{U}^l_{:, r_l}\right) \tag{16}$$

where $\{\mathcal{V}^l\}_{l=1}^m$ (with $\mathcal{V}^l \in \mathbb{R}^{H \times W \times R_l}$) are intermediate results, and $\mathcal{V}^1 \in \mathbb{R}^{H \times W \times R_m}$ is initialized as all zeros and final prediction is returned as $\mathcal{V} = \mathcal{V}^{m+1}$.

Proof of Equation 16 We denote the convolutional tensor-train decomposition in Equation 15 as $\mathcal{T} = \mathsf{CTTD}(\mathcal{T}^l)_{l=1}^m$, then Equation 16 can be rewritten as Equation 17 since $\mathcal{V}^1$ is an all zeros tensor.

$$\mathcal{V}_{:,r_{m+1}} = \sum_{l=1}^{m} \sum_{r_l=1}^{R_l} \mathsf{CTTD}\left(\{\mathcal{T}^t\}_{t=l}^m\right)_{:,r_l,r_{m+1}} * \mathcal{U}^l_{:,r_l} + \sum_{r_1=1}^{R_1} \mathsf{CTTD}\left(\{\mathcal{T}^t\}_{t=1}^m\right)_{:,r_1,r_{m+1}} * \mathcal{V}^1_{:,r_1} \tag{17}$$

$$= \sum_{l=2}^{m} \sum_{r_l=1}^{R_l} \mathsf{CTTD}\left(\{\mathcal{T}^t\}_{t=l}^m\right)_{:,r_l,r_{m+1}} * \mathcal{U}^l_{:,r_l} + \sum_{r_1=1}^{R_1} \mathsf{CTTD}\left(\{\mathcal{T}^t\}_{t=1}^m\right)_{:,r_1,r_{m+1}} * \left(\mathcal{U}^1_{:,r_1} + \mathcal{V}^1_{:,r_1}\right) \tag{18}$$

Note that the second term in Equation 18 can now be simplified as

$$\sum_{r_1=1}^{R_1} \mathsf{CTTD}\left(\{\mathcal{T}^t\}_{t=1}^m\right)_{:,r_1,r_{m+1}} * \left(\mathcal{U}^1_{:,r_1} + \mathcal{V}^1_{:,r_1}\right) \tag{19}$$

$$= \sum_{r_1=1}^{R_1} \left(\sum_{r_2=1}^{R_2} \cdots \sum_{r_m=1}^{R_m} \mathcal{T}^1_{:,r_1,r_2} * \cdots * \mathcal{T}^m_{:,r_m,r_{m+1}} \right) * \left(\mathcal{U}^1_{:,r_1} + \mathcal{V}^1_{:,r_1}\right) \tag{20}$$

$$= \sum_{r_2=1}^{R_2} \left(\sum_{r_3=1}^{R_3} \cdots \sum_{r_m=1}^{R_m} \mathcal{T}^2_{:,r_2,r_3} * \cdots * \mathcal{T}^m_{:,r_m,r_{m+1}} \right) * \left[\sum_{r_m=1}^{R_m} \mathcal{T}^1_{:,r_1,r_2} * \left(\mathcal{U}^1_{:,r_1} + \mathcal{V}^1_{:,r_1}\right) \right] \tag{21}$$

$$= \sum_{r_2=1}^{R_2} \mathsf{CTTD}\left(\{\mathcal{T}^t\}_{t=2}^{m-1}\right)_{:,r_2,r_{m+1}} * \mathcal{V}^2_{:,r_2} \tag{22}$$

where the sequential algorithm in Equation 16 is performed to achieve Equation 22 from Equation 21. Plugging Equation 22 into Equation 18, we reduce Equation 18 back to the form as Equation 17.

$$\mathcal{V}_{:,r_{m+1}} = \sum_{l=2}^{m} \sum_{r_l=1}^{R_l} \mathsf{CTTD}\left(\{\mathcal{T}^t\}_{t=l}^m\right)_{:,r_l,r_{m+1}} * \mathcal{U}^l_{:,r_l} + \sum_{r_2=1}^{R_2} \mathsf{CTTD}\left(\{\mathcal{T}^t\}_{t=2}^{m-1}\right)_{:,r_2,r_{m+1}} * \mathcal{V}^2_{:,r_2} \tag{23}$$

which completes the induction.

B. Model Details, Ablation Studies and Additional Experimental Results

B.1. Model Details

Details of the Architecture. All experiments use a stack of 12-layers of ConvLSTM or Conv-TT-LSTM with 32 channels for the first and last 3 layers, and 48 channels for the 6 layers in the middle. A convolutional layer is applied on top of all LSTM layers to compute the predicted frames, followed by an optional sigmoid function (In the experiments, we add sigmoid for KTH dataset but not for Moving-MNIST-2). Additionally, two skip connections performing concatenation over channels are added between (3, 9) and (6, 12) layers as is shown in Figure 8.

Hyper-parameters Selection Table 4 summarizes our search values

Kernel size	Initial learning rate	Tensor order	Tensor rank	Time steps
$\{3, 5\}$	$\{1e\text{-}4, 5e\text{-}3, 1e\text{-}3\}$	$\{1, 2, 3, 5\}$	$\{4, 8, 16\}$	$\{1, 3, 5\}$

Table 4. Hyper-parameters search values for Conv-TT-LSTM experiments.

B.2. Ablation Studies

Fixed Window Strategy. We investigate the another realization of Conv-TT-LSTM, i.e. a different implementation of Equation (5). With fixed window strategy, all previous steps $\{\mathcal{H}^l\}_{l=1}^n$ are concatenated into a single 3-rd order tensor

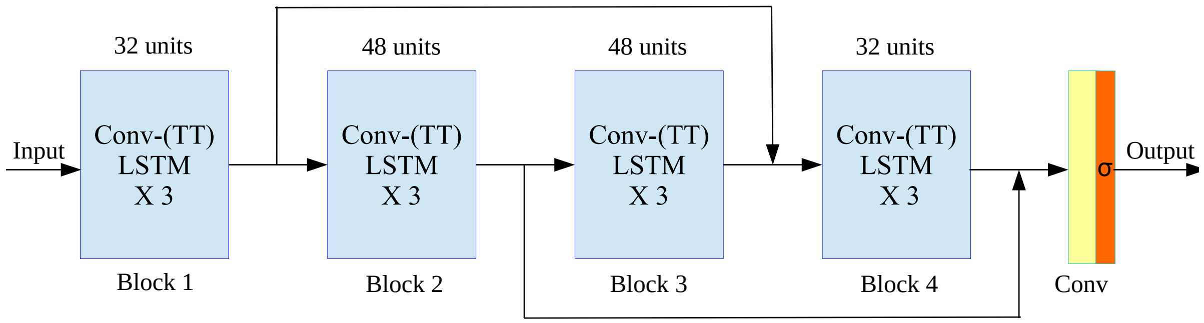

Figure 8. Illustration of the network architecture for the 12-layers model used in the experiments.

$\hat{\mathcal{H}}^t \in \mathbb{R}^{H\times W\times nC}$, which is repeatedly mapped to m tensors $\{\tilde{\mathcal{H}}^{t,o} \in \mathbb{R}^{H\times W\times R}\}_{o=1}^m$ by 2D-convolution with kernels $\{\mathcal{K}^o \in \mathbb{R}^{k\times k\times nC\times R}\}_{o=1}^m$.

$$\textbf{Conv-TT-LSTM (FW):} \quad \tilde{\mathcal{H}}^{t,o} = \mathcal{K}^o * \hat{\mathcal{H}}^t = \mathcal{K}^o * \left[\mathcal{H}^{t-n}; \cdots; \mathcal{H}^{t-1}\right] \tag{24a}$$

$$\textbf{Conv-TT-LSTM (SW):} \quad \tilde{\mathcal{H}}^{t,o} = \mathcal{K}^o * \hat{\mathcal{H}}^{t,o} = \mathcal{K}^o * \left[\mathcal{H}^{t-n+m-l}; \cdots; \mathcal{H}^{t-l}\right] \tag{24b}$$

For comparison, we list the equations for both fixed window and sliding window strategies above. In Table 5, we compare these two realizations on Moving-MNIST-2 under the same experimental setting, and we find that sliding window performs slightly better than fixed window.

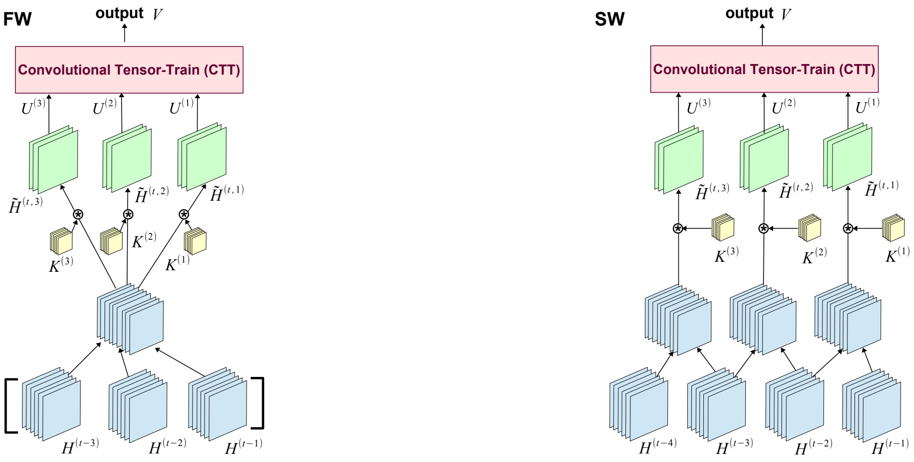

(a) Conv-TT-LSTM (FW)

(b) Conv-TT-LSTM (SW)

Figure 9. Illustration of two realizations of convolutional tensor-train LSTM. **(a)** In **Fixed Window (FW)** realization, all steps are used to compute each input to convolutional tensor-train, while **(b)** in **Sliding Window (SW)** realization, only steps in the window are used for computation at each input.

Ablation Study on our Experiment Setting. To understand whether our proposed Conv-TT-LSTM universally improves upon ConvLSTM (i.e. not tied to specific architecture, loss function and learning schedule), we perform three ablation studies on our experimental setting: **(1)** Reduce the number of layers from 12 layers to 4 layers (same as (Xingjian et al., 2015) and (Wang et al., 2018a)); **(2)** Change the loss function from $\mathcal{L}_1 + \mathcal{L}_2$ to $\mathcal{L}_1$ only; **(3)** Disable the scheduled sampling and use teacher forcing during training process. We evaluate the performance of ConvLSTM baseline and our proposed Conv-TT-LSTM under these ablated settings, and summarize their comparisons in Table 5. The results show that our proposed Conv-TT-LSTM consistently outperforms ConvLSTM for all settings, i.e. the Conv-TT-LSTM model improves upon ConvLSTM in a board range of setups, which is not limited to the certain setting used in our paper. These ablation studies further show that our setup is optimal for predictive learning in Moving-MNIST-2 dataset.

Model		Layers		Sched.		Loss		(10 -> 30)			Params.
		4	12	TF	SS	ℓ_1	$\ell_1 + \ell_2$	MSE	SSIM	LPIPS	
ConvLSTM	-	✓	×	×	✓	×	✓	37.19	0.791	184.2	11.48M
Conv-TT-LSTM	FW							**31.46**	**0.819**	**112.5**	**5.65M**
ConvLSTM	-	×	✓	✓	×	×	✓	33.96	0.805	184.4	3.97M
Conv-TT-LSTM	FW							**30.27**	**0.827**	**118.2**	**2.65M**
ConvLSTM	-	×	✓	×	✓	✓	×	36.95	0.802	135.1	3.97M
Conv-TT-LSTM	FW							**34.84**	**0.807**	**128.4**	**2.65M**
ConvLSTM	-	×	✓	×	✓	×	✓	33.08	0.806	140.1	3.97M
Conv-TT-LSTM	FW							**28.88**	**0.831**	**104.1**	**2.65M**
Conv-TT-LSTM	SW	×	✓	×	✓	×	✓	25.81	**0.840**	**90.38**	2.69M

Table 5. Evaluation of ConvLSTM and our Conv-TT-LSTMs under ablated settings. In this table, FW stands for *fixed window* realization, SW stands for *sliding window* realization; For learning scheduling, TF denotes *teaching forcing* and SS denotes *scheduled sampling*. The experiments show that **(1)** our Conv-TT-LSTM is able to improve upon ConvLSTM under all settings; **(2)** Our current learning strategy is optimal in the search space; **(3)** The sliding window strategy outperforms the fixed window one under the optimal experimental setting.

B.3. Additional Experimental Results

Per-frame metrics for KTH action dataset. The per-frame metrics are illustrated in Figure 10.

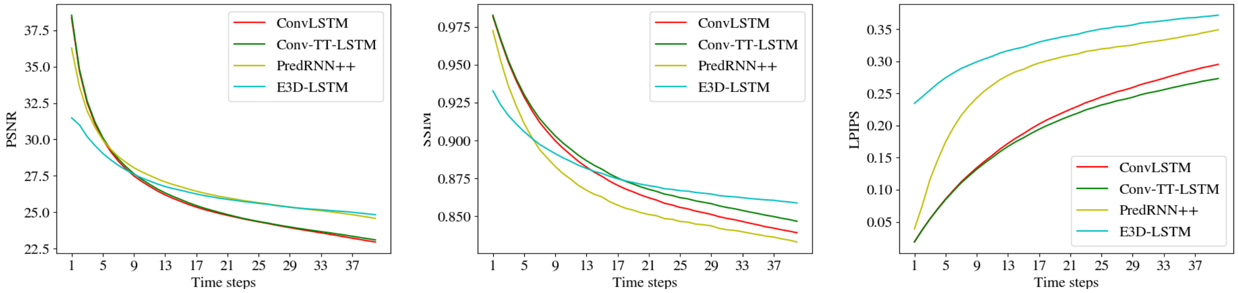

Figure 10. Frame-wise comparison in PSNR, SSIM and PIPS on KTH action dataset. For LPIPS, lower curves denote higher quality; while for PSNR and SSIM, higher curves imply better quality. Our Conv-TT-LSTM performs better than ConvLSTM baseline, PredRNN++ (Wang et al., 2018a) and E3D-LSTM (Wang et al., 2018b) in terms of SSIM and LPIPS.

Additional Visual Results. We provide additional visual comparison among PredRNN++ (Wang et al., 2018a), E3D-LSTM (Wang et al., 2018b), our baseline ConvLSTM and our proposed Conv-TT-LSTM.

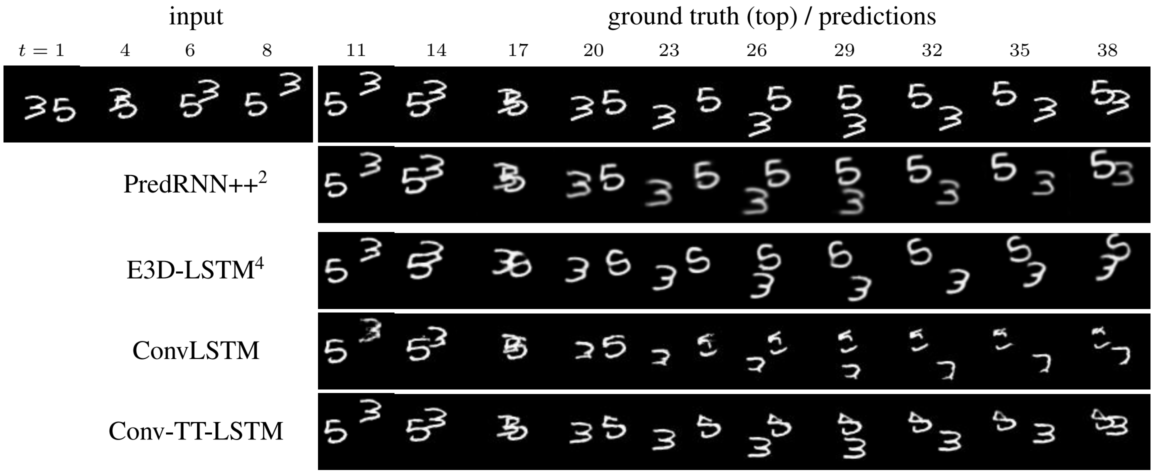

Figure 11. 30 frames prediction on Moving-MNIST given 10 input frames. Every 3 frames are shown. The first frames ($t = 1$ and 11) are animations. To view the animation, Adobe reader is required.

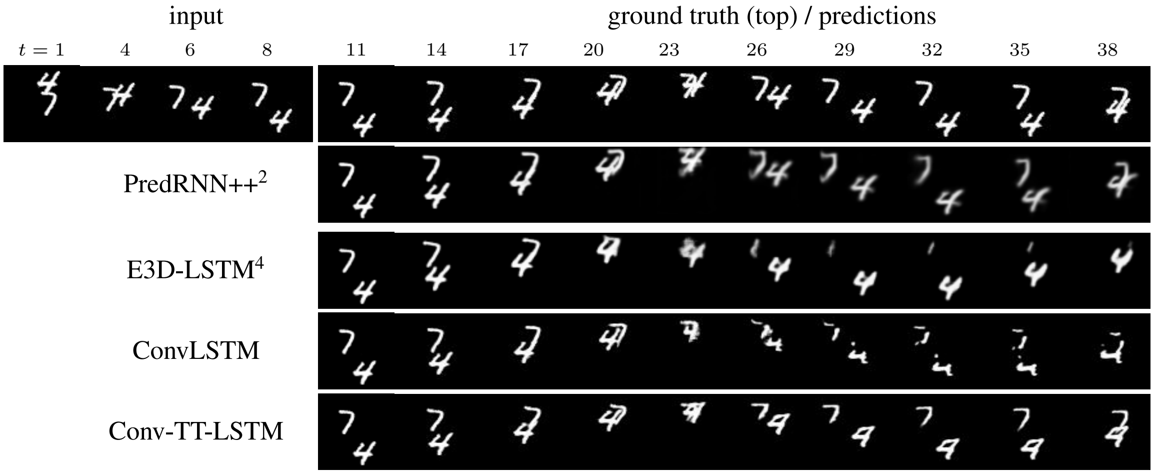

Figure 12. 30 frames prediction on Moving-MNIST given 10 input frames. Every 3 frames are shown. The first frames ($t = 1$ and 11) are animations. To view the animation, Adobe reader is required.

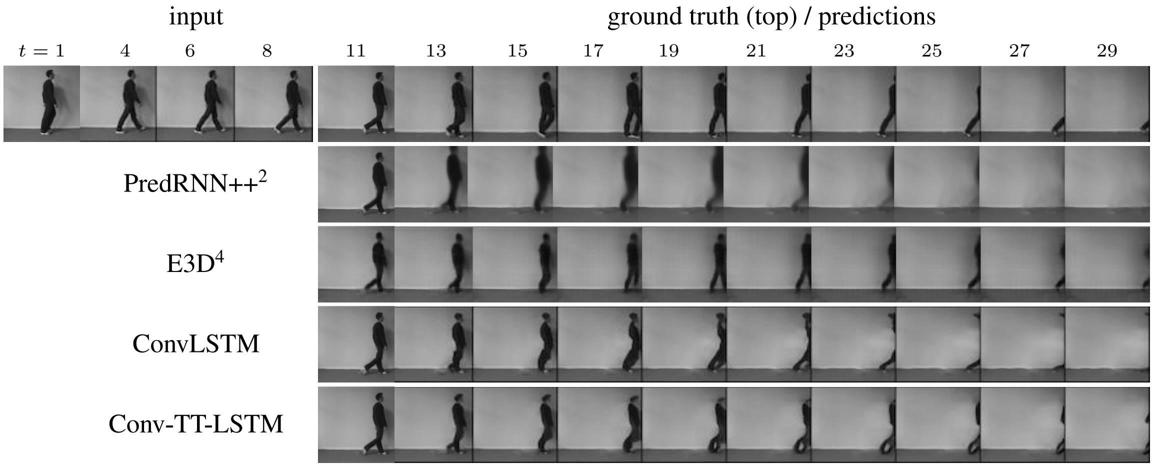

Figure 13. 20 frames prediction on KTH given 10 input frames. Every 2 frames are shown. The first frames ($t = 1$ and 11) are animations. To view the animation, Adobe reader is required.

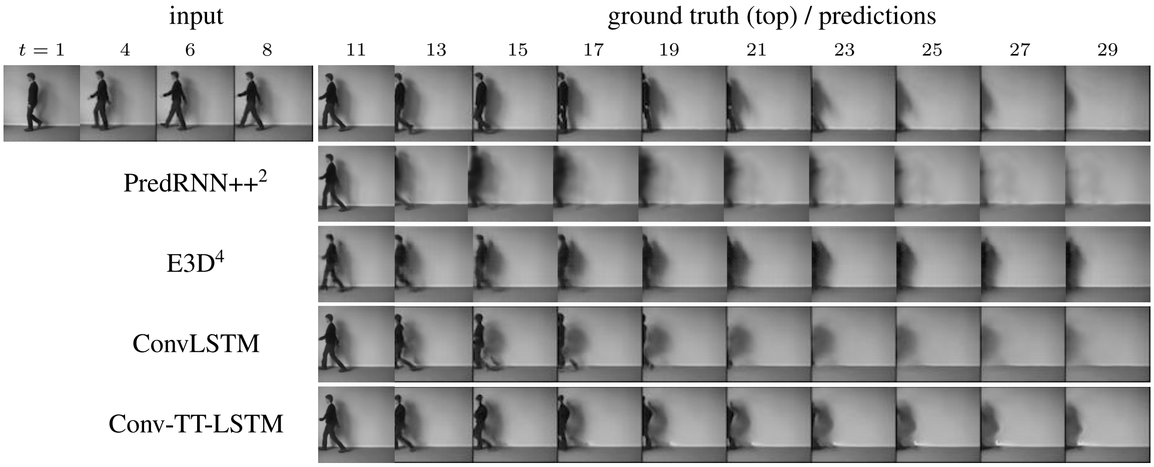

Figure 14. 20 frames prediction on KTH given 10 input frames. Every 2 frames are shown. The first frames ($t = 1$ and 11) are animations. To view the animation, Adobe reader is required.